Electromagnetic Biology and Medicine, 27: 372–385, 2008

ISSN 1536-8378 print/1536-8386 online
DOI: 10.1080/15368370802394644

informa
healthcare

Variability of the Minimal Transmembrane Voltage Resulting in Detectable Membrane Electroporation

LEILA TOWHIDI[1], TADEJ KOTNIK[2], GORAZD PUCIHAR[2], S. M. P. FIROOZABADI[1], HOSSEIN MOZDARANI[3], AND DAMIJAN MIKLAVČIČ[2]

[1]Department of Medical Physics, Tarbiat Modares University, Tehran, Iran
[2]Laboratory of Biocybernetics, Faculty of Electrical Engineering, University of Ljubljana, Ljubljana, Slovenia
[3]Department of Medical Genetics, Tarbiat Modares University, Tehran, Iran

We present a study of the variability of the minimal transmembrane voltage resulting in detectable electroporation of the plasma membrane of spherical and irregularly shaped CHO cells (we denote this voltage by ITVc). Electroporation was detected by monitoring the influx of Ca^{2+}, and the transmembrane voltage was computed on a 3D finite-elements model of each cell constructed from its cross-section images. We found that ITVc was highly variable, particularly in irregularly shaped cells, where it ranged from 512–1028 mV. We show that this range is much too large to be an artifact due to numerical errors and experimental inaccuracies, implying that for cells of the same type and exposed to the same number of pulses with the same duration, the value of ITVc can differ considerably from one cell to another. We also observed that larger cells are in many cases characterized by a higher ITVc than a smaller one. This is in qualitative agreement with the reports that higher membrane curvature facilitates electroporation, but quantitative considerations suggest that the observed variability of ITVc cannot be attributed entirely to the differences in membrane curvature.

Keywords Electroporation; Electropermeabilization; Transmembrane voltage; Transmembrane potential; Membrane curvature.

Introduction

From the electrical perspective, a biological cell consists of an electrolyte (highly conductive) interior surrounded by a thin insulating (almost non conductive) membrane. When exposed to an external electric field, a cell locally distorts it, with the cell interior practically devoid of the field (after the steady state is reached), and with the local field contained almost entirely in the membrane. Equivalently, this is expressed as a potential difference across the membrane—the induced transmembrane voltage (ITV). The ITV is proportional to the external field, as well as to the size of the cell, depends on the shape and orientation of the cell within the field, and varies with the

Address correspondence to Tadej Kotnik, Laboratory of Biocybernetics, Faculty of Electrical Engineering, University of Ljubljana, Ljubljana, Slovenia; E-mail: tadej.kotnik@fe.uni-lj.si

position on the membrane (Pauly and Schwan, 1959; Marszalek et al., 1990; Kotnik et al., 1997; Kotnik and Miklavčič, 2000a,b, 2006). An increase of the ITV results in a higher probability of various structural changes in the membrane, particularly the formation of aqueous pores (Weaver and Chizmadzev, 1996; Kakorin et al., 1996; Neumann et al., 1999). Using appropriate electric field pulse parameters, this phenomenon, referred to as electroporation or electropermeabilization, is transient and reversible. The method is nowadays widely used in biotechnology (Teissie et al., 2002; Faurie et al., 2005) and in medical applications such as electrochemotherapy (Heller et al., 1999; Serša et al., 2003; Gothelf et al., 2003; Mir, 2006), gene electrotransfer (Dean, 2005, Golzio et al., 2005), and transdermal drug delivery (Denet et al., 2004; Pliquett and Weaver, 2007).

Although aqueous pore formation is strictly speaking not a threshold phenomenon, the increase of membrane electric conductivity and permeability to otherwise non permeant molecules only become detectable if the pulse amplitude, and thus the ITV, is sufficiently large (Rols and Teissié, 1990; Weaver and Chizmadzev, 1996). Experiments confirm that electroporation first becomes detectable in those regions of the cell membrane where the ITV is the highest, and only if it exceeds a certain critical value, which will henceforth be denoted as ITVc (Hibino et al., 1993; Gabriel and Teissié, 1997; Miklavčič et al., 2006). In many applications, knowledge of the value of ITVc can contribute to a successful application of electroporation.

Since the ITV is proportional to the cell size and depends on the cell orientation in the field, large cells and cells elongated in the direction of the field are typically porated at lower pulse amplitudes than smaller cells and cells elongated in the direction perpendicular to the field (Valič et al., 2003). However, whether ITVc as the more fundamental quantity (with respect to the pulse amplitude) is itself variable has to our knowledge not yet been subjected to a systematical investigation.

In several studies, it was implicitly assumed that—at least for cells of the same type and exposed to the same number of pulses having the same duration—ITVc is a constant, which facilitated modeling and simulation (Hibino et al., 1993; Bier, 2002; Pucihar et al., 2006; Zudans et al., 2007; Puc et al., 2003). In some studies, ITVc was also evaluated experimentally by determining the minimal applied electric field at which electroporation of some cells in the sample became detectable (Teissié and Rols, 1993; Čegovnik and Novaković, 2004). This provided an estimate of the ITVc on the largest cell (or several of the largest cells) in the sample, but it did not address the possibility of ITVc being variable within the cell population.

There are several theoretical arguments in favor of ITVc being to some extent variable. First, studies of lipid vesicles of various sizes suggest that because of the different packing density of the lipid molecules in the two monolayers of strongly curved membranes, these appear to be electroporated easier (i.e., have a lower ITVc) than planar membranes (Neumann et al., 1999; Kakorin et al., 2003; Tönsing et al., 1997). These differences become pronounced for spherical vesicles with radii below 200 nm (Kakorin et al., 2003) and for irregularly shaped cells with correspondingly large local curvatures. Consequently, with spherical cells the role of curvature on the ITVc should be negligible (as their radii are in tens of μm), while with irregularly shaped cells characterized by a sufficiently high local curvature, this effect could be significant.

Second, theoretical considerations also suggest that ITVc is affected by rigid membrane inclusions with inherent anisotropic curvature (Fošnarič et al., 2003; Kandušer et al., 2003). As a consequence, ITVc in cells containing such inclusions could perhaps be different from ITVc in cells devoid of them.

The relation between the field amplitude and the percentage of electroporated cells in an exposed sample is typically a sigmoidally shaped curve (Teissié and Rols, 1993; Kandušer et al., 2003). This does not in itself imply that ITVc is variable, and Puc et al. (2003) showed that this curve shape largely reflects the distribution of cell sizes in the sample. However, there was a detectable discrepancy between their experimental results and the predictions of their theoretical model based solely on cell size distribution, which could be attributed to a variability of ITVc.

The aim of our study was to investigate the variability of ITVc within a population of roughly spherical cells, and within a population of irregularly shaped cells, with pulses of the same duration used in all experiments. For this purpose, we combined experimental determination of electroporation with numerical computation of the ITV. The cell models used in computation were built from cross-section images of the same cells on which electroporation were performed, thus reflecting their actual geometry and orientation with respect to the external field.

Materials and Methods

Cells

Chinese hamster ovary cells (CHO-K1) were grown in their native culture medium HAM-F12 (Dulbecco's modification of the Eagle's Minimum Essential Medium—EMEM) supplemented with 8% fetal calf serum, 0.15 mg/ml L-glutamine (all three from Sigma-Aldrich, Steinheim, Germany), 200 units/ml benzylpenicillin (penicillin G), and 16 μg/mg gentamicin and incubated in 5% CO_2 at 37°C.

The cells were plated in Lab-Tek II chambers (Nalge Nunc International, USA) at 2×10^4 cells per chamber. Experiments on irregularly shaped cells were performed 22–24 h after the plating, when the cells were firmly attached to the surface of the chamber (see Figures 1 and 2). Experiments on spherical cells were performed 2–3 h after the plating, as this time was sufficient for the cells to adhere to the surface with only a small region of the membrane, but still remain roughly spherical (see Figure 3). Only the cells sufficiently far apart as to not influence the ITV on each other were considered (see Figure 1 and the remark in the caption).

Preparation of the cells for the experiments was performed in three consecutive steps:

1. The cells were washed with Spinner's Minimum Essential Medium (SMEM, Gibco, USA; a calcium-depleted modification of EMEM), kept at 21°C for 30 min in SMEM containing 1.5 μM Fura2-AM (Grynkiewicz et al., 1985) and 200 μM pluronic acid (both from Molecular probes, Leiden, Netherland), and subsequently washed again with SMEM. Fura2-AM enters the cell through an intact membrane, and is transformed in the cytosol into Fura2, the active and membrane-non permeant ratiometric calcium-sensitive dye (excitation 340/380 nm, emission 540 nm). Subsequent washing removed Fura2-AM from the extracellular medium.
2. SMEM containing 10 μM di-8-ANEPPS (Molecular Probes, Leiden, Netherlands) was added, and the cells were kept for 10 min at 4°C. At this temperature, internalization of the dye through an intact plasma membrane, e.g., by endocytosis, is largely inhibited. Subsequently cells were washed again with SMEM. During this time, di-8-ANEPPS, which is a potentiometric membrane marker (excitation 490 nm, emission 605 nm), bound to the plasma membrane of the cells, making the cell

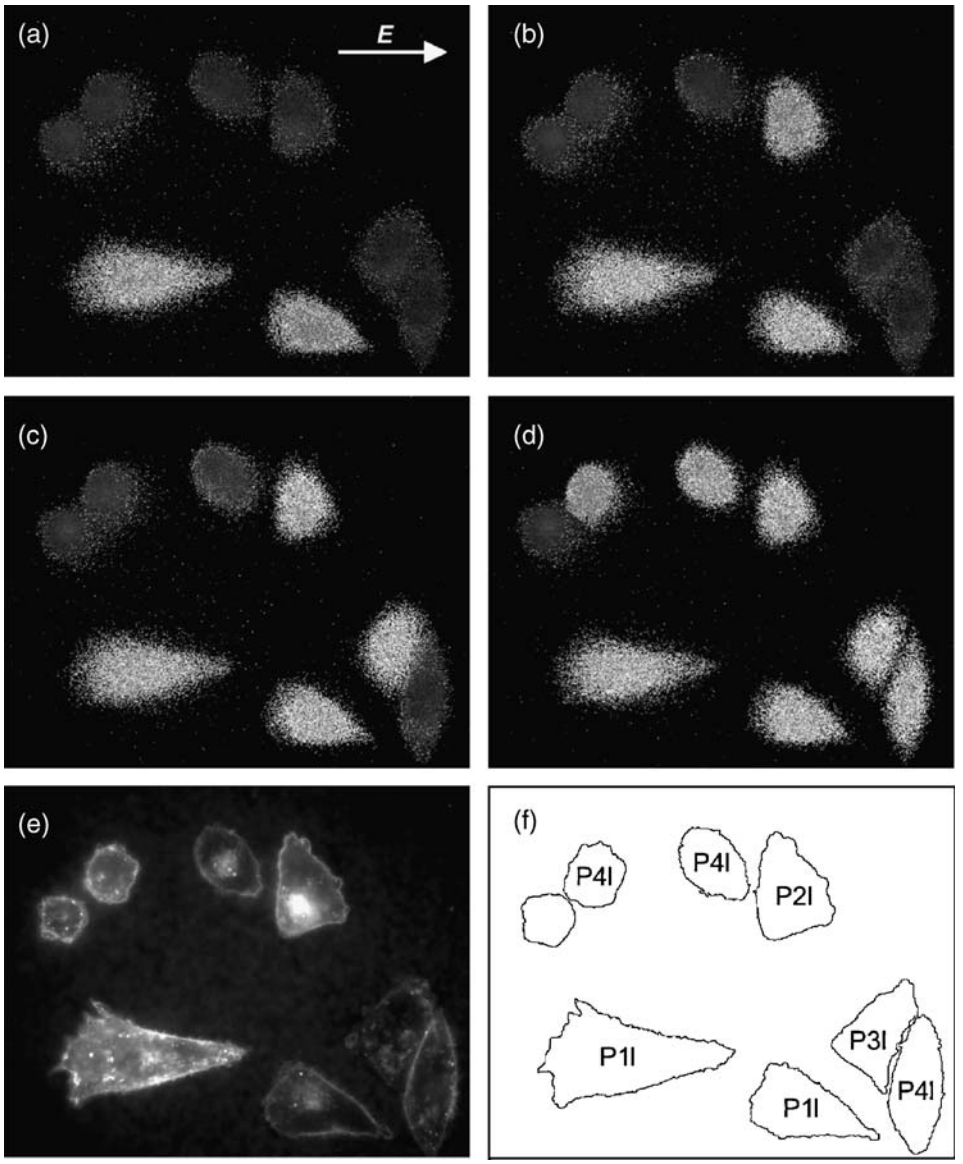

Figure 1. (a)–(d) Electroporation detected by intracellular Fura2. (e) Cell edges detected by di-8-ANEPPS. (f) Contours of the cells and their classification into sets P2I, P3I, and P4I. This is an illustrative example as it shows cells belonging to each of the sets, but in the actual experiments the cells in close contact, such as the pair of the cells in the bottom right corner of (a)–(d), were excluded from the analysis as they mutually affect the local field and thus the ITV on each other.

edges visible for the whole duration of the experiment. Subsequent washing removed di-8-ANEPPS from the extracellular medium.

3. Finally, SMEM was replaced with the native culture medium HAM-F12, which contains a 1.05 mM concentration of Ca^{2+} ions. Thus, the calcium ions were present in the extracellular medium but nearly absent from the cytosol, as they do not readily cross an intact (non porated) cell membrane. At the same time, the

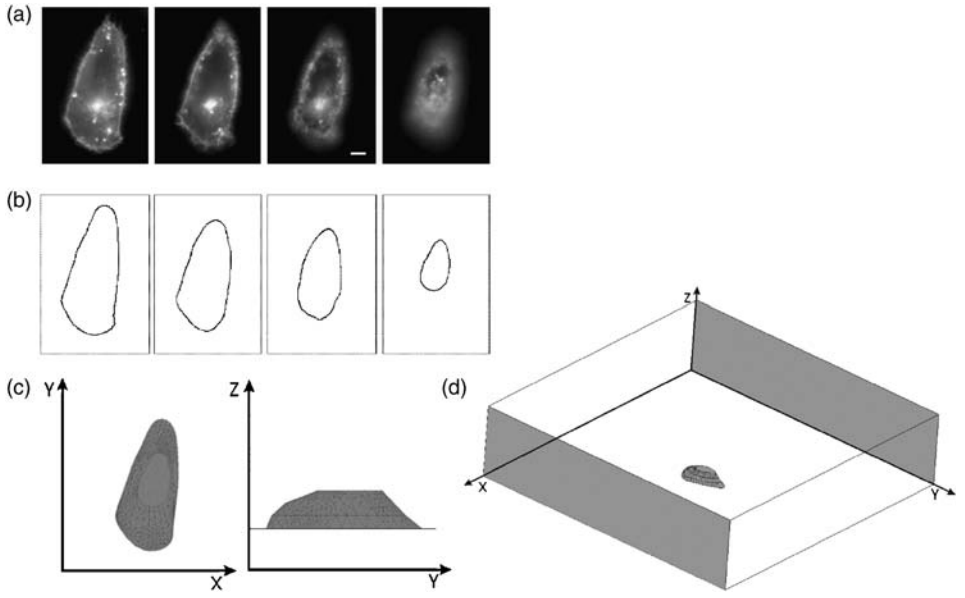

Figure 2. (a) Four cross-sections of a CHO cell, from the bottom up, in vertical increments of 2 μm. The bar corresponds to 5 μm. (b) The contours. (c) The top and side views of the 3D cell model. (d) The positioning of the cell model and the electrodes (the gray surfaces).

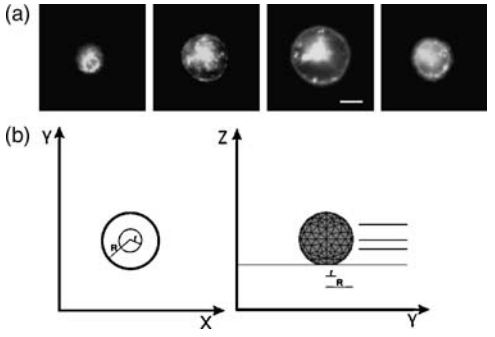

Figure 3. (a) Four cross-sections of a typical CHO cell considered as spherical, from the bottom up, at the levels of 0, 4, 6, and 10 μm. The bar corresponds to 5 μm. (b) The top and side views of the cell model; $R = 6.4\,\mu m$, $r = 2.3\,\mu m$. The horizontal lines correspond to the cross-section levels.

Ca^{2+} indicator Fura2 was contained in the cytosol, providing the means for detection of electroporation, which resulted in influx of Ca^{2+} ions into the cytosol.

Detection of Electroporation—General

A pair of parallel Pt/Ir wire electrodes with 0.8 mm diameter and 4 mm distance between them was positioned at the bottom of the chamber, in which the level of the medium was 3 mm. The electric potential distribution was computed for this geometry

and realistic electrical properties, showing that the field was highly homogeneous in the central region between the electrodes. Therefore, all the cells considered in our study were chosen from this region. The electric pulses were generated by the Cliniporator device (IGEA s.r.l., Carpi, Modena, Italy).

Electroporation resulted in the entry of Ca^{2+} ions into the cells, where their binding to Fura2 caused the change of its emission spectra for the two excitation wavelengths. The presence of calcium was determined ratiometrically, with the excitation wavelengths set at 340 nm and 380 nm, and the emission measured at 540 nm for both excitation wavelengths. This method provides sufficient sensitivity for detecting intracellular levels of free Ca^{2+} as low as 100 nM. As the extracellular Ca^{2+} concentration was five decimal orders of magnitude higher (1.05 mM), the influx of Ca^{2+} ions caused by permeabilization was easily discerned from the background.

Detection of Electroporation—The Experimental Concept

While experimental and numerical determination of the ITV on the cell under consideration are relatively straightforward tasks, determination of the ITVc is much more challenging, particularly if the same pulse duration and number of pulses are to be used for each cell studied. Namely, in principle ITVc could be determined by exposing the cell to a ramp-shaped pulse, with the amplitude steadily increasing until electroporation would become detectable, but in such an experiment different cells would be subjected to exposures of differing durations, and as ITVc is known to be affected by pulse duration, the results of such a study would be of little use.

An alternative is to use a sequence of pulses with constant duration, but with incrementing amplitudes. In general, this procedure is also flawed, as ITVc is also known to be affected by the number of pulses applied. This effect is less pronounced with longer delays between consecutive pulses. However, an excessively long exposure (e.g., hours) to the conditions required for electroporation and its detection, primarily the presence of the dyes, is detrimental for the cells and could thereby affect the results. In addition, unlike for the ramp, when using a sequence of pulses, one cannot exclude the possibility that the cells electroporated already by the first pulse (i.e., the one with the lowest amplitude) would be porated by a pulse with an even lower amplitude.

Taking these considerations into account, we exposed each sample of cells to a sequence of four rectangular 100 μs pulses, delivered one after another with delays of 4 min, and with pulse amplitudes incrementing by 20 V (or equivalently, with the voltage-to-distance ratio incrementing by 50 V/cm). The cells for which electroporation was detected already by the first pulse applied were omitted from further analysis. The cells that were porated by the second pulse but not by the first were categorized into the set P2S for spherical and P2I for irregularly shaped cells, those porated by the third but not the second into P3S and P3I, and similarly for P4S and P4I. This allowed us to consider the variability of ITVc separately for each set. Figure 1 shows a sample of cells electroporated and classified using this procedure.

To ensure that cells of various shapes and sizes were represented in each of the three P-sets, the amplitude of the first pulse was varied from one repetition of the experiment to another, with values ranging from 60–240 V (from 150–600 V/cm). The procedure was continued until the sets P2I, P3I, and P4I each consisted of 33 cells, and sets P2S, P3S, and P4S each consisted of 22 cells.

Finite-Elements Model and Computation of ITV and ITVc

The 3D finite-elements model of the cell was built from cross-section fluorescence images obtained by shifting the focus of the fluorescence microscope (AxioVert 200, $\times 63$ objective with oil immersion, Zeiss, Germany) vertically in constant steps of 2 μm from the bottom to the top of the cells. The images were acquired with a cooled VisiCam 1280 CCD camera and MetaMorph 7.0 software (both Visitron, Germany). The cell contours were determined in Corel PhotoPaint 11.0 (Corel Corp., Ottawa, Canada) and converted into 3D objects using MATLAB 7.2 (MathWorks Inc., Natick, MA, USA) and FEMLAB 3.3 (COMSOL Inc., Burlington, MA). The procedure, illustrated in Figure 2, is described in more detail in Pucihar et al. (2006). The fluorescence in the cell interior reflects partial relocation of di-8-ANEPPS from the plasma membrane to the cytosol and its binding to organelle membranes.

For spherical cells, the contours were used to verify whether the cell shape was indeed sufficiently close to spherical. For the cells qualifying, the model was constructed as a sphere flattened at the bottom, with the radius equal to the largest measured radius among the circular cross sections. Figure 3 shows one typical example of this procedure.

To avoid the problems related to building the very thin cell plasma membrane from finite elements, the membrane was instead modeled as a boundary condition, as explained in detail in Pucihar et al. (2006). The extracellular and intracellular regions were constructed separately and connected using the pair feature in COMSOL. Adaptive mesh size was used, with finer mesh in the vicinity of the membrane and coarser farther away. The total number of mesh elements in each simulation was around 20,000.

The conductivities of the cytoplasm and the (non porated) membrane were set at 3×10^{-1} S/m and 5×10^{-7} Sm^{-1}, respectively, and the membrane thickness at 5 nm (Kotnik et al., 1997; Kotnik and Miklavčič, 2006). The conductivity of the extracellular medium was set at 1 S/m, as measured by a conductometer (MA5950, Metrel, Horjul, Slovenia) for HAM-F12 medium.

The electric field was generated by assigning fixed potentials to two opposite faces of a rectangular chamber with dimensions of $200 \times 200 \times 50$ μm (see Figure 2).

For each cell, the ITV was computed in COMSOL 3.3 (COMSOL Inc., Burlington, MA) using the Conductive Media DC Mode of the AC/DC Module, and with the applied (external) electric field strength equal to the voltage-to-distance ratio that led to the first electroporation of the cell under consideration.

The computation in COMSOL yielded the distribution of electric potential throughout the model, and the distribution of ITV on the membrane was then computed as the potential drop at the boundary between the cytosol and the cell exterior. The value of ITVc was determined as the maximal value of the ITV (Figure 4).

Results and Discussion

In Figure 5, we show the dependence of ITVc on cell radius for the spherical cells in sets P2S, P3S, and P4S. As this figure shows, there was a significant variability of ITVc, with the larger spherical cells generally porated at higher ITVc than smaller ones. This is in qualitative agreement with the theoretical prediction that ITVc should be lower at higher membrane curvature. However, both theoretical and experimental considerations suggest that the impact of membrane curvature on membrane electroporation is highly pronounced for radii in the range of tens of nm, and then decreases with increase

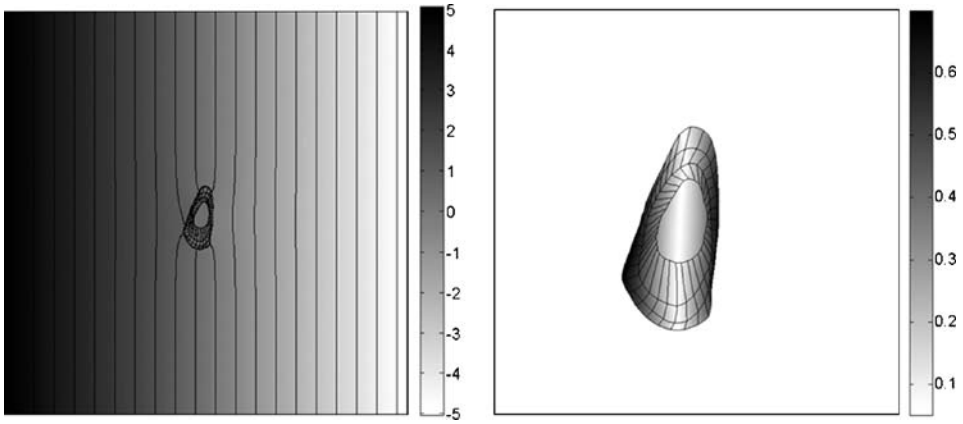

Figure 4. (Left) The computed electric potential (in volts) in the cell interior and exterior for the lowest cross-section in Figure 2. The curves are the equipotentials. (Right) The absolute value of the ITV (in volts) on the cell membrane computed as the electric potential drop at the boundary between the cytosol and the cell exterior.

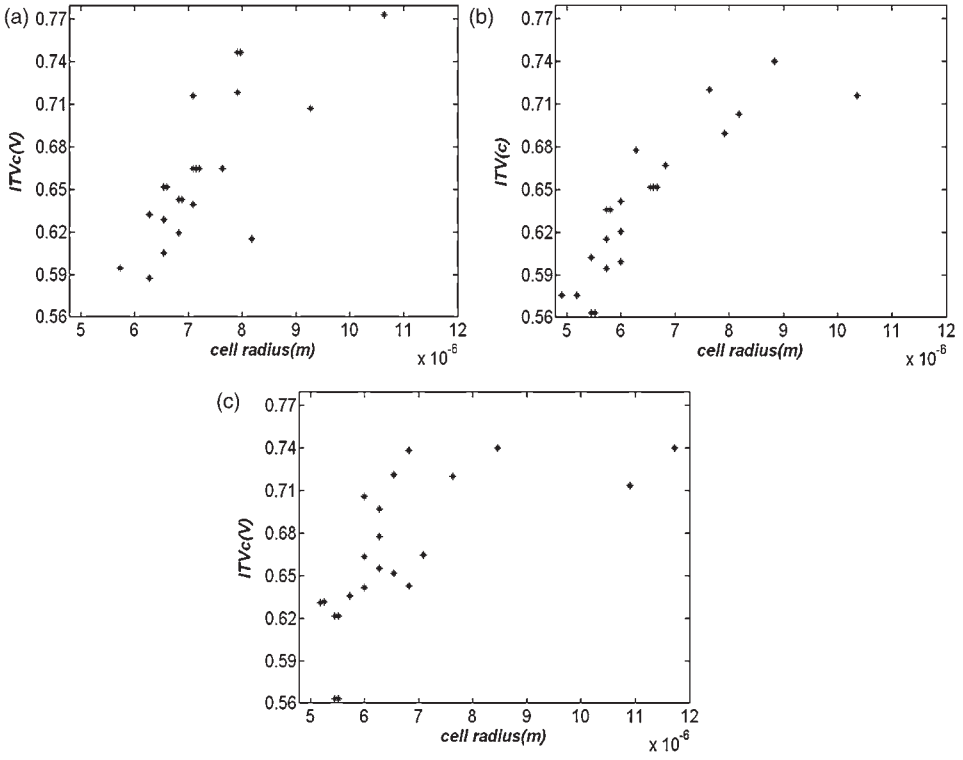

Figure 5. The effect of cell radius on ITVc. (a) In the set P2S, (b) in P3S, and (c) in P4S.

of the radius (Kakorin et al., 2003). Therefore, it is questionable whether the membrane curvature itself could affect the ITVc of spherical biological cells, as their radii are in the range of several μm. As among the cells of a clonogenic cell line the main reason for differences in cell size is the different stage of their cell cycle, this suggests that changes

occurring in the membrane during the cycle could perhaps contribute to the observed tendency of larger cells having a higher ITVc than smaller ones.

In smaller cells, the same Ca^{2+} influx results in a higher concentration of internalized Ca^{2+}, making electroporation easier to detect than in larger cells. In principle, this could lead to apparently lower ITVc values detected in smaller than in larger cells. However, if this would be the main reason for the observed variability of ITVc, then there would be no vertical scattering in Figure 5, where all the cells on a single vertical have the same size. Moreover, electroporation was typically characterized by a prominent increase in fluorescence, as seen in Figure 1.

In Figure 6, these same data presented in Figure 5 are shown in histograms indicating the distribution of ITVc for populations of spherical cells in each of the three sets. In each set, the maximal observed ITVc is about 30% larger than the

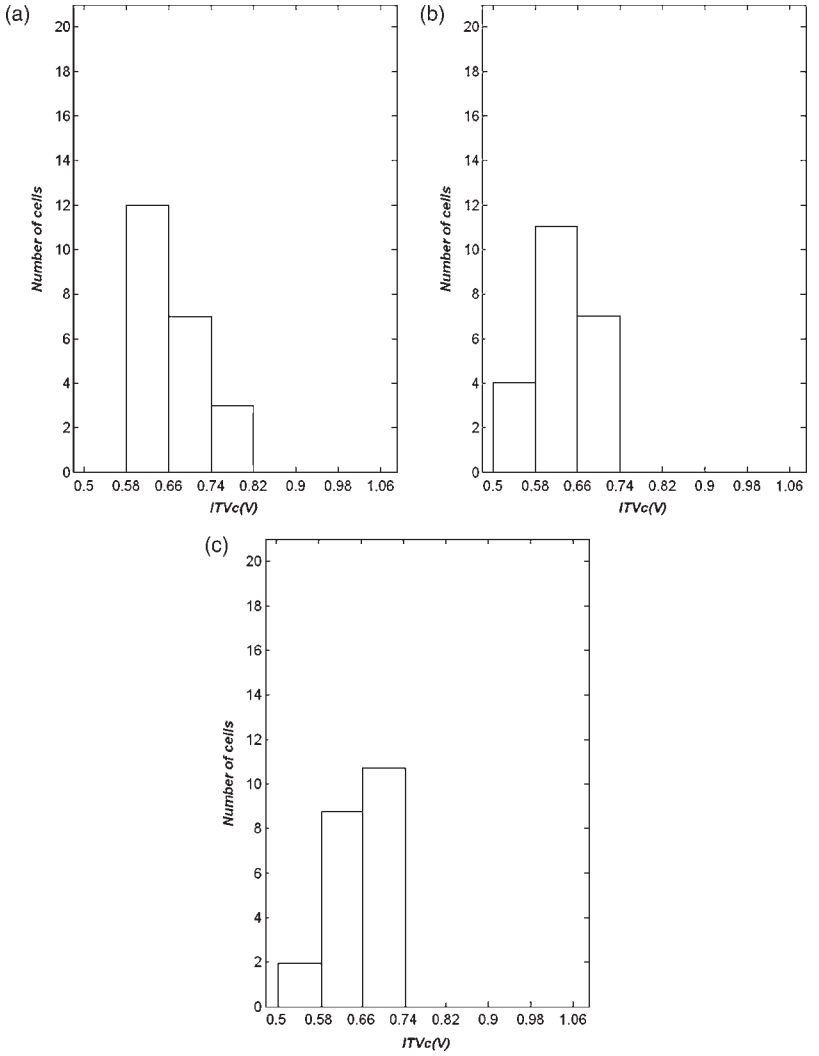

Figure 6. The distribution of ITVc for the spherical cells. (a) In the set P2S, (b) in P3S, and (c) in P4S, with each set containing 22 cells.

minimal one, which is roughly in agreement with the differences reported in some previous studies (Gabriel and Teissié, 1997), and in contrast with the assumption that ITVc is a constant. The shapes of the distributions in the P2S, P3S, and P4S also apparently differ, but the statistical significance of these differences is questionable due to the relatively small size of the samples.

The results obtained for irregularly shaped cells are illustrated, in analogy to Figure 6, in the three histograms in Figure 7 corresponding to P2I, P3I, and P4I, and also showing the top views of the 3D models of all the cells. Similar to the case of spherical cells, here we observed a significant variability of ITVc as well, with larger cells in many cases porated at higher ITVc than smaller ones. In fact, the ITVc distribution for irregularly shaped was even considerably broader than for spherical

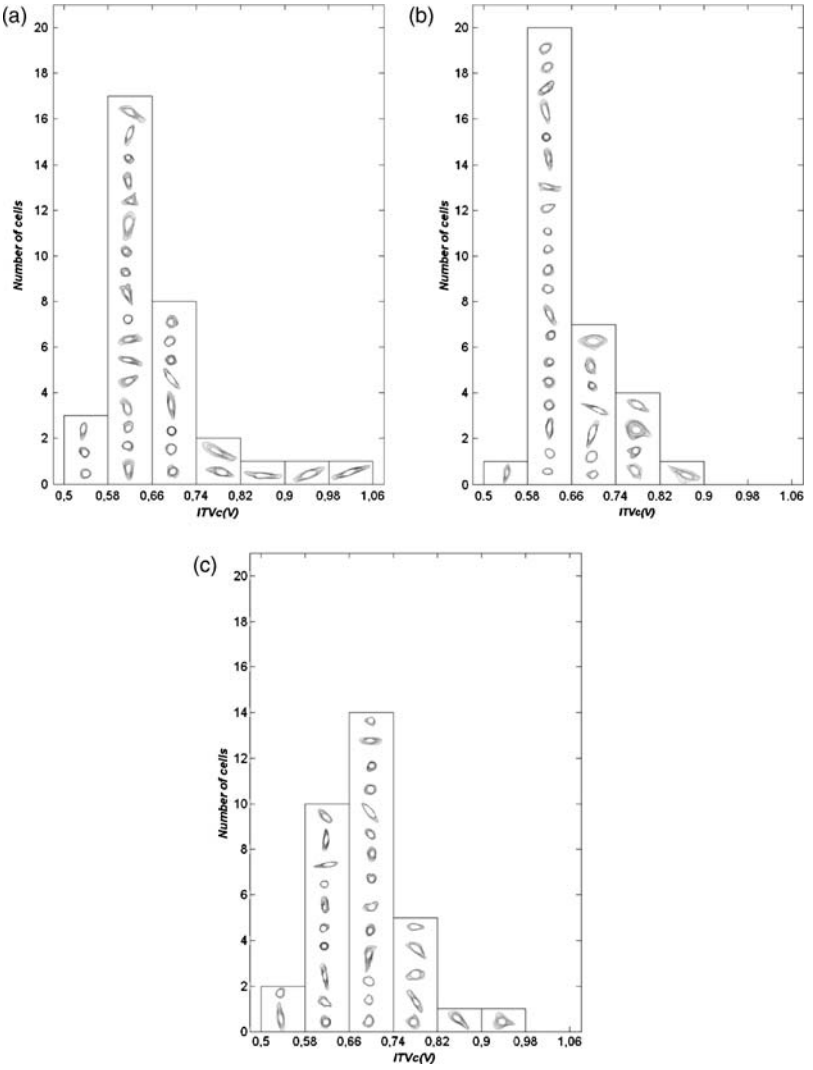

Figure 7. The values of ITVc for the attached cells. (a) In the set P2I, (b) in P3I, and (c) in P4I, with each set containing 33 cells, and with the top view of the 3D cell models shown (the applied electric field was directed from left to right).

cells. For example, for the three sets treated together, the minimal ITVc is 512 mV, and the maximal 1028 mV, which is more than 100% higher. Also, for each individual set, this difference is larger than 75%. As we elaborate in the subsequent paragraphs, this variability is much too large to be attributable entirely to errors and inaccuracies.

In general, local membrane curvature in certain regions of an irregularly shaped cell can be much higher than the membrane curvature of the spherical cells. Therefore, in irregularly shaped cells the effect of membrane curvature on ITVc could be much more pronounced than in spherical cells, thereby contribute to the observed larger variability of ITVc in irregular cells. Still, some of the largest cells that were characterized by very high ITVc were also highly elongated in the direction of the field, displaying a relatively high curvature in the membrane regions exposed to the highest ITV (sharp cell endings facing the electrodes; see the rightmost columns of the three histograms in Figure 7). This seems to be in contrast with the expectation that ITVc should be lower for higher membrane curvature.

We should note that the general observation of larger cells having a higher ITVc is not in contrast with the well-known empirical observation that large cells and cells elongated in the direction of the field are typically porated at the lowest pulse amplitudes (Valič et al., 2003). This can be seen in Figure 1, and more clearly in Figure 8, which shows the same cells as Figure 7, but with the pulse amplitude plotted on the horizontal axis instead of the ITVc.

There are in general four possible sources of the deviations between the actual and the computed values of ITVc: (i) the deviation between the actual shape of the cell and the shape of its 3D model; (ii) the errors of the numerical computation; (iii) the inaccuracy due to the discretized increase of pulse amplitude; and (iv) the imprecision in distinguishing porated and non porated cells based on their fluorescence. We now consider each of these contributions separately in more detail:

1. As Figure 2 shows, the clarity of the outline was not identical for all cross sections. Furthermore, for merging the model contours into a solid body the contours had to consist of the same number of line segments, irrespective of the size and the complexity of the actual cell contour. It is difficult to evaluate precisely the maximal error in the computation of ITV and ITVc due to the deviation between the shape of the cell and the model, but it is important to note that in our study we only considered the cells for which the lowermost contour was very clearly visible. Namely, this is also the contour that affects the ITV distribution most importantly, and which in almost all cases contains the point with ITVc. Based on the experience gained through computing ITV on a large number of cell models, we estimate that the maximal error due to inaccuracies in the modeling itself cannot exceed 30 mV.
2. A detailed analysis of the numerical method applied here for computation of ITV (see Section 2.4) was performed previously (Pucihar et al., 2006). This analysis suggests that with the mesh accuracy used in our study and with induced voltages of the same magnitudes, the error due to the numerical method does not exceed 20 mV, and is typically much smaller than this.
3. For precise determination of ITVc, the amplitude of the external electric field would have to increase continuously. As in our experiment it instead increased in steps of 50 V/cm, the ITV also increased in steps, with the increment depending on the particular cell shape and size. Among the cells considered in this study, this increment never exceeded 147 mV, and for the majority of the cells it was below 100 mV.

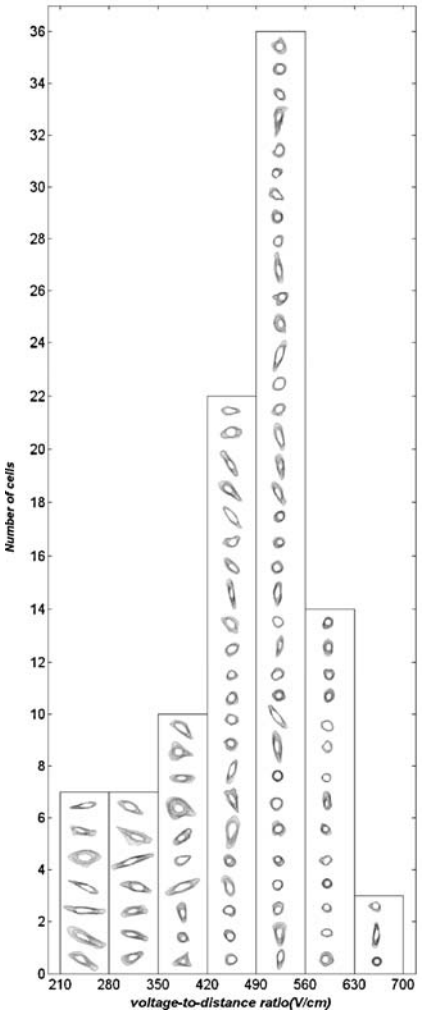

Figure 8. The lowest pulse amplitude (expressed as the ratio between the voltage and the distance between the plate electrodes) leading to detectable electroporation of the attached cells. The same cells are shown as in Figure 7, with the sets P2I, P3I, and P4I merged into a single set.

4. In the majority of cases, the porated cells were clearly distinguishable from non porated ones based on their intensity observed in the ratiometric image. In some cases, however, this intensity was weak, but still stronger than for the typical non porated cells, while the subsequent pulse with higher amplitude resulted in obvious poration. For these cases, we had to set a threshold intensity for categorizing a cell as porated. This choice was made based on experience, but was to some extent arbitrary, and thereby introduced another possible inaccuracy, which by the reasoning given in the preceding paragraph could not exceed 147 mV.

In summary, even the worst-case scenario in which all the errors analyzed above would be maximal and point in the same direction, the total error in our determination of ITVc could not exceed 344 mV.

Moreover, it is difficult to envisage that the errors 3 and 4 would combine; if for a pulse of a given amplitude it is unclear whether electroporation occurred, electroporation with an even lower pulse amplitude is even less likely. In fact, the weak intensity was never observed for two consecutive pulse amplitudes.

Taking this into consideration, we can conclude that the maximal realistic error in our determination of ITVc could not exceed $\pm$ 197 mV. With the values of ITVc spanning from 512–1028 mV, the differences can therefore not be an artifact entirely due to errors and inaccuracies. Together with the results obtained on spherical cells, this implies that for cells of the same type and exposed to the same number of pulses with the same duration, the value of ITVc can differ considerably from one cell to another. Further investigations will be required to elucidate the mechanisms underlying the observed variability of ITVc.

Acknowledgment

This work was supported by the Slovenian Research Agency. Leila Towhidi wishes to thank the Faculty of Electrical Engineering of the University of Ljubljana, Slovenia, for their hospitality during this research.

References

Bier, M. (2002). Resealing dynamics of a cell membrane after electroporation. *Phys. Rev. E* 66:062905.

Čegovnik, U., Novaković, S. (2004). Setting optimal parameters for in vitro electrotransfection of B16F1, SA1, LPB, SCK, L929 and CHO cells using predefined exponentially decaying electric pulses. *Bioelectrochemistry* 62:73–82.

Dean, D. A. (2005). Nonviral gene transfer to skeletal, smooth, and cardiac muscle in living animals. *Amer. J. Physiol. Cell. Physiol.* 289:C233–C245.

Denet, A. R., Vanbever, R., Préat, V. (2004). Skin electroporation for transdermal and topical delivery. *Adv. Drug Deliv. Rev.* 56:659–674.

Faurie, C., Golzio, M., et al. (2005). Electric field induced cell membrane permeabilization and gene transfer: theory and experiments. *Eng. Life Sci.* 5:179–186.

Fošnarič, M., Kralj-Iglič, V., et al. (2003). Stabilization of pores in lipid bilayers by anisotropic inclusions. *J. Phys. Chem. B* 107:12519–12526.

Gabriel, B., Teissié, J. (1997). Direct observation in the millisecond time range of fluorescent molecule asymmetrical interaction with the electropermeabilized cell membrane. *Biophys. J.* 73:2630–2637.

Golzio, M., Mazzolini, L., et al. (2005). Inhibition of gene expression in mice muscle by *in vivo* electrically mediated siRNA delivery. *Gene Ther.* 12:246–251.

Gothelf, A., Mir, L. M., Gehl, J. (2003). Electrochemotherapy: results of cancer treatment using enhanced delivery of bleomycin by electroporation. *Cancer Treat. Rev.* 29:371–378.

Grynkiewicz, G., Poenie, M., Tsien, R. Y. (1985). A new generation of Ca^{2+} indicators with greatly improved fluorescence properties. *J. Biol. Chem.* 260:3440–3450.

Heller, R., Gilbert, R., Jaroszeski, M. J. (1999). Clinical applications of electrochemotherapy. *Adv. Drug Deliv. Rev.* 35:119–129.

Hibino, M., Itoh, H., Kinosita, K. Jr. (1993). Time courses of cell electroporation as revealed by submicrosecond imaging of transmembrane potential. *Biophys. J.* 64:1789–1800.

Kakorin, S., Liese, T., Neumann, E. (2003). Membrane curvature and high-field electroporation of lipid bilayer vesicles. *J. Phys. Chem. B* 107:10243–10251.

Kakorin, S., Stoylov, S. P., Neumann, E. (1996). Electro-optics of membrane electroporation in diphenylhexatriene-doped lipid bilayer vesicles. *Biophys. Chem.* 58:109–116.

Kandušer, M., Fošnarič, M., et al. (2003). Effect of surfactant polyoxyethylene glycol (C12E8) on electroporation of cell line DC3F. *Colloid Surf. A* 214:205–217.

Kotnik, T., Bobanović, F., Miklavčič, D. (1997). Sensitivity of transmembrane voltage induced by applied electric fields—a theoretical analysis. *Bioelectrochem. Bioenerg*. 43:285–291.

Kotnik, T., Miklavčič, D. (2000a). Analytical description of transmembrane voltage induced by electric fields on spheroidal cells. *Biophys. J*. 79:670–679.

Kotnik, T., Miklavčič, D. (2000b). Second-order model of membrane electric field induced by alternating external electric fields. *IEEE Trans. Biomed. Eng*. 47:1074–1081.

Kotnik, T., Miklavčič, D. (2006). Theoretical evaluation of voltage inducement on internal membranes of biological cells exposed to electric fields. *Biophys. J*. 90:480–491.

Marszalek, P., Liu, D. S., Tsong, T. Y. (1990). Schwan equation and transmembrane potential induced by alternating electric field. *Biophys. J*. 58:1053–1058.

Miklavčič, D., Čorović, S., et al. (2006). Importance of tumour coverage by sufficiently high local electric field for effective electrochemotherapy. *Eur. J. Cancer Suppl*. 4:45–51.

Mir, L. M. (2006). Bases and rationale of the electrochemotherapy. *Eur. J. Cancer Suppl*. 4:38–44.

Neumann, E., Kakorin, S., Tönsing, K. (1999). Fundamentals of electroporative delivery of drugs and genes. *Bioelectrochem. Bioenerg*. 48:3–16.

Pauly, H., Schwan, H. P. (1959). Über die Impedanz einer Suspension von kugelförmigen Teilchen mit einer Schale. *Z. Naturforsch*. 14B:125–131.

Pliquett, U., Weaver, J. C. (2007). Feasibility of an electrode-reservoir device for transdermal drug delivery by noninvasive skin electroporation. *IEEE Trans. Biomed. Eng*. 54:536–538.

Puc, M., Kotnik, T., et al. (2003). Quantitative model of small molecules uptake after in vitro cell electropermeabilization. *Bioelectrochemistry* 60:1–10.

Pucihar, G., Kotnik, T., et al. (2006). Numerical determination of transmembrane voltage induced on irregularly shaped cells. *Ann. Biomed. Eng*. **34** :642–652.

Rols, M. P., Teissié, J. (1990). Electropermeabilization of mammalian cells: quantitative analysis of phenomenon. *Biophys. J*. 58:1089–1098.

Serša, G., Čemažar, M., Rudolf, Z. (2003). Electrochemotherapy: advantages and drawbacks in treatment of cancer patients. *Cancer Ther*. 1:133–142.

Teissié, J., Rols, M. P. (1993). An experimental evaluation of the critical potential difference inducing cell membrane electropermeabilization. *Biophys. J*. 65:409–413.

Teissié, J., Eynard, N., et al. (2002). Recent biotechnological developments of electropulsation: a prospective review. *Bioelectrochemistry* 55:107–112.

Tönsing, K., Kakorin, S., et al. (1997). Annexin V and vesicle membrane electroporation. *Eur. Biophys. J*. 26:307–318.

Valič, B., Golzio, M., et al. (2003). Effect of electric field induced transmembrane potential on spheroidal cells: theory and experiment. *Eur. Biophys. J*. 32:519–528.

Weaver, J. C., Chizmadzev, Y. A. (1996). Theory of electroporation: a review. *Bioelectrochem. Bioenerg*. 41:135–160.

Zudans, I., Agarwal, A., et al. (2007). Numerical calculations of single-cell electroporation with an electrolyte-filled capillary. *Biophys. J*. 92:3696–3705.